tdLanYFP, a yellow, bright, photostable and pH insensitive fluorescent protein for live cell imaging and FRET-based sensing strategies.

Bousmah Y.[a], Valenta H.[a], Bertolin G.[b], Singh U. [a], Nicolas V.[c], Pasquier H.[a], Tramier M.[b], Merola F.[a], Erard M[a].

[a]Université Paris-Saclay, CNRS, Institut de Chimie Physique, 91405 Orsay, France

[b]Univ Rennes, CNRS, IGDR [(Institut de génétique et développement de Rennes)] – UMR 6290, 35000 Rennes, France

[c]Microscopy Facility (MIPSIT), Ingénierie et Plateformes au Service de l'Innovation Thérapeutique – IPSIT – UMS – US31 – UMS3679 (IPSIT), Université Paris-Saclay, 92296 Châtenay-Malabry, France

Abstract

Yellow fluorescent proteins (YFP) are widely used as optical reporters in Förster Resonance Energy Transfer (FRET) based biosensors. Although great improvements have been done, the sensitivity of the biosensors is still limited by the low photostability and the poor fluorescence performances of YFPs at acidic pHs. In fact, today, there is no yellow variant derived from the EYFP with a $pK_{1/2}$ below ~5.5. Here, we characterize a new yellow fluorescent protein, tdLanYFP, derived from the tetrameric protein from the cephalochordate *B. lanceolatum*, LanYFP. With a quantum yield of 0.92 and an extinction coefficient of 133 000 $mol^{-1}.L.cm^{-1}$, it is, to our knowledge, the brightest dimeric fluorescent protein available, and brighter than most of the monomeric YFPs. Contrasting with EYFP and its derivatives, tdLanYFP has a very high photostability *in vitro* and preserves this property in live cells. As a consequence, tdLanYFP allows the imaging of cellular structures with sub-diffraction resolution with STED nanoscopy. We also demonstrate that the combination of high brightness and strong photostability is compatible with the use of spectro-microscopies in single molecule regimes. Its very low $pK_{1/2}$ of 3.9 makes tdLanYFP an excellent tag even at acidic pHs. Finally, we show that tdLanYFP can be a FRET partner either as donor or acceptor in different biosensing modalities. Altogether, these assets make tdLanYFPa very attractive yellow fluorescent protein for long-term or single-molecule live-cell imaging that is also suitable for FRET experiment including at acidic pH.

Acknowledgement

This work has benefited from the SpICy microscopy facility of ICP for TSCPC-FLIM measurements, the Microscopy Rennes Imaging Centre (MRic) for FCS and FastFLIM measurements, the Plateforme d'Imagerie Cellulaire MIPSIT for STED measurements and the Light Microcopy Facility Imagerie-Gif for confocal microscopy. We thank P. Pernot for the analysis of the fluorescence decays.

Funding :

This work was supported by LabEx PALM Grant ANR-10-LABX-0039-PALM and by the IDEX Paris Saclay (IRS BioProbe). H.V. was supported by a PhD felloship form MESRI.

The authors declare that they have no conflicts of interest with the contents of this article.

Introduction

Fluorescent proteins (FPs) have become indispensable tools in quantitative imaging to explore cellular chemistry (ion concentrations, membrane potential, molecular crowding) and cell signaling pathways. FPs are used as optical reporters in various biosensing modalities and in particular in the ones taking advantage of the Förster Resonance Energy Transfer (FRET) phenomenon [1]. For FRET, a pair of donor/acceptor FPs is in fact required, with the fluorescence spectrum of the donor overlapping the absorption one of the acceptor [2]. If the donor and the acceptor are fused to two proteins of interest, FRET can be used to probe protein-protein interactions [3]. It is also possible to genetically fuse the donor and the acceptor on both sides of a sensing module to build the so-called FRET biosensors which are useful tools to monitor variations in ion or metabolite concentrations [1] or to follow numerous enzymatic activities[4] in living cells. The sensitivity and the reliability of FRET-based biosensors depend on the specifications of the donor/acceptor pair. Ideally, FPs should display controlled and simple photophysical behavior with a mono-exponential fluorescence decay and limited excited-state reactions in complex environments such as in living cells, which would ensure an accurate monitoring of the biological event of interest. The sensitivity of the detection is also directly linked to the total number of photons collected per FP's fluorophore. This number depends first on the ability of the protein to express and to mature efficiently towards a fluorescent chromophore. It relies also on the molecular brightness of the protein that is the product of the extinction coefficient and the fluorescence quantum yield of the chromophore. Finally, the total photon budget of a given FP depends on its propensity to irreversibly photobleach upon illumination.

In most FRET experiments (~60%), a cyan FP is chosen as a donor and a yellow one as an acceptor [5]. Tsien's laboratory originally developed the historical ECFP / EYFP pair, which is still in use nowadays in certain biosensors [6]. Nevertheless, both FPs suffer from several drawbacks as a relatively low brightness, a complex photophysics and a strong pH sensitivity for ECFP, while EYFP exhibits mainly strong pH and chloride sensitivities. Substantial efforts were made to improve their performances over the past 20 years. For cyan fluorescent proteins, ECFP variants with lower sensitivity to their environment, efficient maturation, high brightness including an optimized quantum yield close to 1, and very good photostability have been available for several years (Aquamarine [7], mTurquoise [8], mTurquoise2 [9]). The best ones notably display a low $pK_{1/2}$, the pH value, at which 50% of the fluorescence is lost, down to 3.1, which is compatible with detection of biological events in the acidic environment [5]. This feature opens new opportunities to develop FRET-based biosensors dedicated to the real-time visualization

of metabolic activities in acidic environments, whether it is due to local pH variations or due to their localization in intracellular compartments [10], including secretory vesicles [11] or phagocytic vesicles [12].

On the side of the acceptor, EYFP served as a template for several rounds of engineering leading to improved versions of yellow FPs as the popular mCitrine [13,14] or mVenus [15] and Citrine2 [16]. Citrine, the first variant of EYFP released, is much less sensitive to chloride ions and pH than EYFP but unfortunately displays a poor photostability [13]. Years later, the improvement of the photostability of mCitrine lead to Citrine2, which additionally retained a high brightness [16]. Despite all these efforts, none of the yellow variants derived from EYFP are compatible with the reporting of biochemical processes in an acidic environment so far , their $pK_{1/2}$ ranging from 5.3 to 6 [16–18]. Consequently, no FRET biosensors based on a cyan/yellow pair were developed for measurements in acidic environment, the pH sensitivity of the yellow acceptor being still too high [19].

LanYFP, a yellow FP from *Branchiostoma lanceolatum*, attracted our attention due to its very low $pK_{1/2}$ ($pK_{1/2\ LanYFP}$ = 3.5) [17]. LanYFP is tetrameric and has been intensively engineered to lead to the blue-shifted variant mNeonGreen [17,20]. The pH sensitivity of the resulting mNeonGreen is equivalent to that of mCitrine ($pK_{1/2,mNeonGreen}$ ~5.4-5.7) [17,18]. Yet, mNeonGreen has a better photostability in wide field microscopy, the time to loose half of its fluorescence intensity being 3 to 10 time longer for mNeonGreen than mCitrine under the same irradiation conditions depending on the illumination power [17,18]. mNeonGreen's brightness is also slightly better (~ 1.5 times) than all available yellow variants [17,18]. Following these observations, we became interested in the potential offered by the intermediate dimeric version, dLanYFP, obtained along the genetic engineering of mNeonGreen from the natural tetrameric LanYFP. Here, we present a complete characterization of dLanYFP *in vitro* and evaluate the potentialities given by its tandem version tdLanYFP for live-cell imaging. Especially, we highlight its performance as FRET partner in genetically encoded biosensors even at acidic pH, and its suitability for super-resolution microscopy thanks to its very high photostability.

Results and discussion

Biochemical parameters and fluorescence characterization of dLanYFP

dLanYFP was produced in *E. coli* and purified according to standard protocols for fluorescent proteins. Although it is expressed as a monomer, a strong spontaneous dimer formation was observed on SDS-PAGE, and these dimers dissociated only by heating the sample 10 min at 90°C (Fig. 1A). We have compared the spectroscopic properties of purified dLanYFP to those of the widely used yellow fluorescent proteins (YFPs), EYFP, Citrine and Venus. The absorption and fluorescence spectra of dLanYFP are almost equivalent to those of the standard YFPs, with a slight blue shift of the absorption and emission maxima by 3 nm and 8 nm respectively (Fig. 1B, Table 1). Therefore, dLanYFP can directly replace standard YFPs without adaptation of spectral selections in any experimental setup. Its molar extinction coefficient, estimated per monomer with the BCA assay, is 133 000 $mol^{-1}.L.cm^{-1}$ and its quantum yield 0.92 (Table 1). The relative brigthness of the fluorophore in dLanYFP is thus improved by nearly a factor of two compared to EYFP, which is remarkable considering that their chromophores are strictly identical, both being constituted by the tripeptide Gly-Tyr-Gly. dLanYFP, together with its tetrameric parent LanYFP, thus ranges among the brightest fluorescent proteins known today. In live cells, we can anticipate that the strong dimer formation by dLanYFP will double the quantity of labeling fluorophores, leading to a potential 4-fold gain in brightness for fluorescence imaging, as compared to tagging with conventional monomeric YFPs. The fluorescence decays of the purified proteins were acquired using the time-correlated single-photon counting (TCSPC) technique upon excitation at 515 nm (Fig. S1, Table 1). For Venus, Citrine and EYFP, the decays are well fitted by near-single exponentials (> 92-94% of the amplitude), with lifetimes in the range of 3 ns consistent with litterature [21]. The decay of dLanYFP is also mostly mono-exponential (> 97%), with a lifetime in a similar range (2.9±0.1 ns). Interestingly, the decay of dLanYFP also includes a small contribution of a negative, very short component, not present in other YFPs, and whose proportion depends on the emission wavelength, suggesting some fast reaction in the excited-state (Fig. S1).

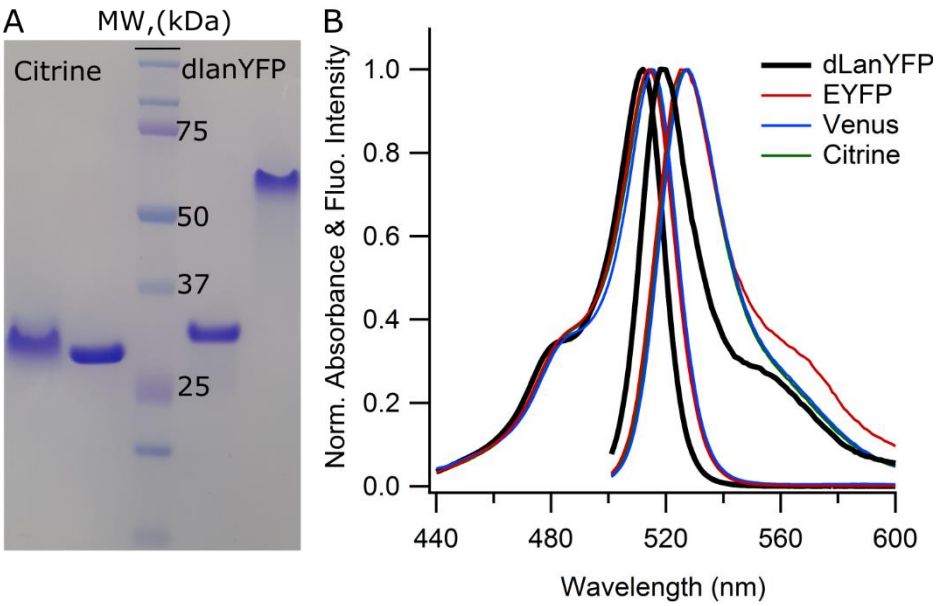

Figure 1: (A) SDS-PAGE of purified Citrine (Lanes 1 and 2) and dLanYFP (Lanes 4 and 5). Lane 1 and 5 samples were not heated whereas lane 2 and 4 samples were heated 10 min at 90°C (Size Marker Dual Color, Biorad). (B) Normalized absorption and emission spectra of dLanYFP, EYFP, Venus and Citrine. Emission spectra were recorded with excitation at 515 nm.

Table 1: *In vitro* characterization of YFPs.

	dLanYFP	**EYFP**	**Venus** **(EYFP F46L-F64L-M153T-V163A-S175G)**	**Citrine** **(EYFP Q69M)**
λ_{max} excitation (nm) λ_{max} emision (nm)	512 519	514 527	515 528	515 527
Extinction coefficient per chain ($mol^{-1}Lcm^{-1}$)	133000±8000[1]	84000±5000	107000±6400	91000±5500
Quantum Yield	0.92±0.05	0.79±0.05	0.78±0.05	0.83±0.05
Rel. Brightness per chain	1.84	1	1.27	1.08
Average fluorescence lifetime[2] (± 0.1 ns)	2.9[3]	3.2	2.9	3.3
pK ½ (± 0.1), $[Cl^-]$ = 85 mM[4]	3.9	6.6	5.9	5.7
Chloride affinity K_{app} (mM)[5]	135±40	70±20	> 250	> 300
Photobleaching decay time (s) agarose beads[6]	687±15	102±20	49±10	37±10
Photobleaching decay time (s) live cells[6]	463±15	44±5	ND	22±5

1 : for one monomer

2 : exc 515nm, em 580nm, 20°C, pH8.

3 : neg. exponent 0.19ns, 3%@ em 535nm, <0.5%@em 580 nm

4 : values obtained with the processing of the absorption spectra

5 : affinities are the average of the values obtained from the fits of the data obtained from the processing of the absorption and the fluorescence spectra

6 : under constant wide-field illumination ex 500 nm, em 542 nm, 0.4W/cm^2

The irreversible photobleaching rate of dLanYFP was compared with the ones of other purified YFPs immobilized on agarose beads (Fig. 2A, Table 1). Under a constant illumination into their major absorption band performed with a wide field microscope, the fluorescence intensity decrease was much slower for dLanYFP in comparison to the other YFPs. dLanYFP appeared to be 15–20 times more photostable than the commonly used Venus and Citrine, making this new YFP very attractive for challenging imaging applications under intense and/or prolonged illumination.

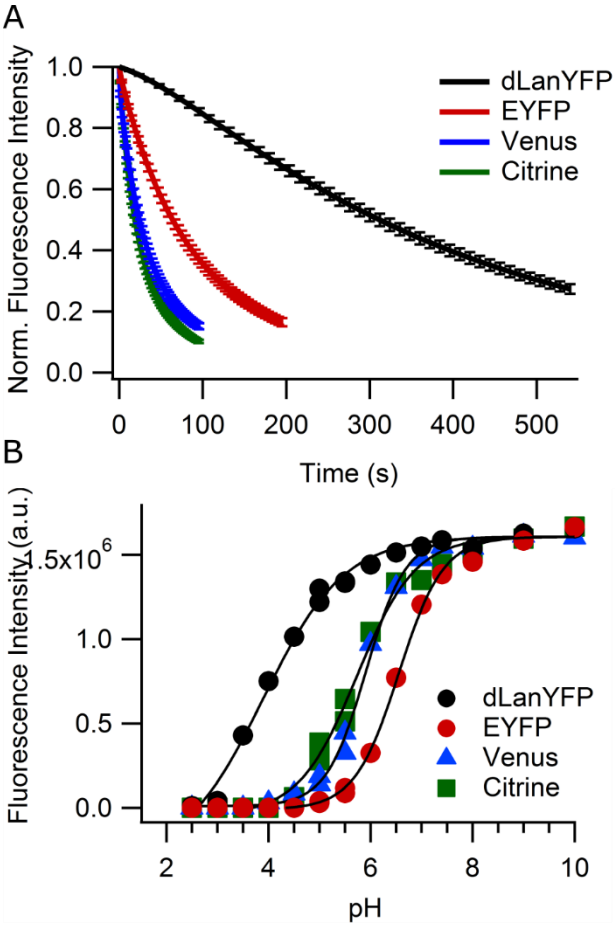

Figure 2: (A) Irreversible photobleaching of YFPs under continuous irradiation in wide-field illumination (0.4 W/cm²). FPs are fixed on Ni^{2+}-NTA agarose beads through their His-tag. Solid lines correspond to the best fits to an exponential analytical model. (B) pH dependence of the fluorescence intensity excited at 480 nm and detected at their maximal emission. Solid lines correspond to the best fits to a sigmoidal analytical model. Experimental data were normalized to 100% maximum of their analytical fits.

The YFP's chomophore contains a phenol moiety that exists both in the protonated and deprotonated form, the latter one being the fluorescent form. It has been shown that $pK_{1/2}$ depends on chloride ion concentration, which can undergo large variations in biological systems. This interdependence of pH and chloride concentration on fluorescence emission intensity was strongly reduced in Citrine by limiting the accessibility of the halide-binding cavity through the introduction of a Met in position 69 instead of a Gln [13]. We compared the $pK_{1/2}$ of dLanYFP with the ones of the YFPs for different choride ion concentrations in the medium (Fig. 2B, Table 1 and Fig. S2). Consistently with the litterature, the $pK_{1/2}$ of EYFP depends strongly on the chloride concentration and are higher than the ones of Citrine and Venus [13,17,22]. For dLanYFP, the $pK_{1/2}$ also depends on the choride ion concentration but is significantly lower whatever the [Cl^-] concentration is in comparison to Citrine, leading to a

$pK_{1/2}$ of 3.9±0.1 at 85 mM [Cl^-], an unprecedented value for a YFP, consistent with the low $pK_{1/2}$ of 3.5 of its parent, LanYFP [17].

Finally, we also evaluated the maturation kinetics of dLanYFP in comparision to the one of Citrine. It was slower (Fig. S3), while remaining in the same order of magnitude or faster than the best CFPs [7]. It is likely that the dimeric character of dlanYFP slowed down the maturation rate compared to the monomeric mNeonGreen [21]. Such phenomenon was also reported for DsRed and its dimeric and monomeric derivatives [23].

The tandem version, tdLanYFP: from expression in live cells to applications in spectro-microscopy

The strong dimerization tendency of dLanYFP might have deleterious consequences in live-cell imaging, by forcing non-physiological intermolecular interactions of its fusion constructs. On the other hand, the introduction of further monomerizing mutations into mNeonGreen resulted in substantially degraded biochemical and photophysical properties [17]. An alternative strategy consists in promoting the formation of a very stable intramolecular dimer of the fluorescent protein, by adequately concatenating two copies of the gene, as was previously done for example with dTomato [24]. A tandem version of dLanYFP, tdLanYFP, was obtained by inserting a 19 amino-acid linker between the two dLanYFP gene copies, by analogy with other existing FP dimers (Fig. S4) [23,24]. To evaluate the tendency of tdLanYFP to oligomerize, the organized smooth endoplasmic reticulum (OSER) assay was performed first in comparison with mCitrine (Citrine A206K) [25]. COS7 cells were transfected with plasmids that express FPs in the Cytoplasmic Endoplasmic Reticulum Membrane (CytERM-FP) and the percentage of cells presenting whorled structures of endoplasmic reticulum triggered by FP oligomerization was evaluated. Typical examples of OSER positive cases for both proteins are shown in Figure S5. For mCitrine, our evaluation of 95% non-OSER situations is consistent with the litterature [18] and shows that dimerization has been efficiently inhibited in this FP variant. For the tandem, the score of 62% non-OSER cases is in the same range as for tdTomato, (57%), and it overcomes Citrine (36%) [18]. Correct localization of tdLanYFP expression in live cells was verified by expressing the protein alone (Fig. 3A), or in fusion with signal peptides targeting the protein to the plasma membrane (Fig. 3B) or the cytoskeleton (Fig. 3C). We also fused tdLanYFP to the C-terminus of $p67^{phox}$, a cytosolic protein belonging to the NADPH oxidase complex that is responsible for the superoxide anion production in many cell types [26]. A representative fluorescence lifetime image (FLIM) of COS7 cells expressing the fusion p67-tdLanYFP and the corresponding fluorescence decay are presented in Figure 3D and 3E. The

average fluorescence lifetime of tdLanYFP fused to this cytosolic protein is similar to that of the purified protein recorded *in vitro* (less than 3% of variation) showing little influence of the fusion on this photophysical parameter.

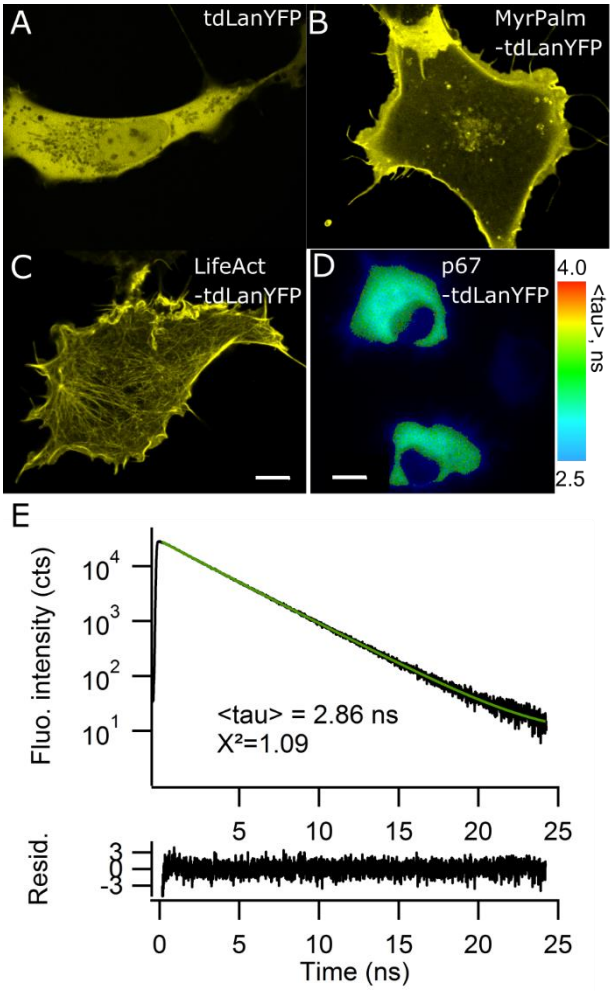

Figure 3: Fluorescence imaging and TCSPC fluorescence decays of tdLanYFP in COS7 cells. Confocal microscopy images of tdLanYFP targeted to the cytosol (A), membrane (B) and cytoskeleton (C). Scale bar 10 µm. (D) Intensity (gray scale) and fluorescence lifetime (color scale) image of a fusion p67-tdLanYFP. Scale bar 15 µm. (E) Fluorescence photons collected from the upper cell were used to calculate the corresponding fluorescence decay. The decay was best fitted with a biexponential fit function (green). The residuals of the fit are displayed below the decay.

We then explored the photostability of tdLanYFP in live cells and confirmed, along wide-field and confocal imaging, its high photostability compared to Citrine and EYFP (Fig. 4). Under wide-field illumination, the characteristic time constants recorded in the cell cytosol are close to the one obtained *in vitro* (Table 1). In confocal imaging, we used cells expressing FPs fused to the actin targeting sequence, LifeAct, to avoid any diffusion between the recording of two successive frames. Again, tdLanYFP was more photostable than mCitrine and bleached 2 to 3

times slower (Fig. 4B). The rates of irreversible photobleaching are known to highly depend on the excitation regimes and it is not surprising to observe a difference between (i) homogeneous and continuous wide field excitation and (ii) the more intense confocal regime where a laser is transiently focused on a single pixel.

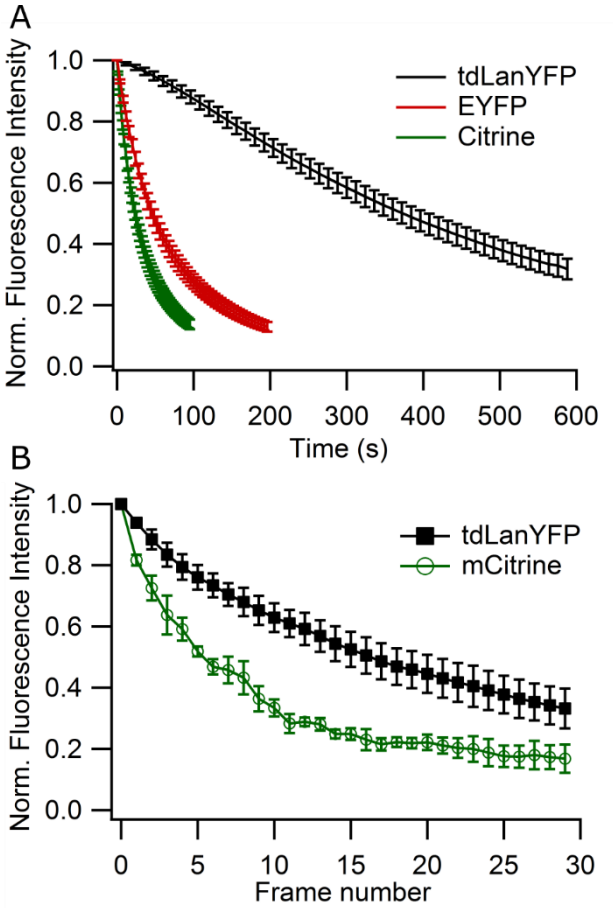

Figure 4: Irreversible photobleaching of YFPs in live COS7 cells. (A) Decay of the fluorescence intensity of COS7 cells expressing cytosolic tdLanYFP, EYFP or Citrine under continuous irradiation in wide-field illumination (0.4 W/cm²). Solid lines correspond to the best fits to an exponential analytical model. Each point is the average of 5 to 10 cells. (B) Decay of the fluorescence intensity of COS7 cells expressing LifeAct-tdLanYFP or LifeAct-mCitrine during a 30-frame time-lapse acquired by confocal microscopy (Average power measured during the scanning on the objective 1,2 µW). Each point is the average of 5 ROIs.

Owing to this high photostability, we decided to evaluate the performances of tdLanYFP in super-resolution imaging. We imaged LifeAct-tdLanYFP transiently expressed in COS7 cells using stimulated-emission-depletion (STED) microscopy (Fig. 5). Due to the cell movements between 2 frames, the tracking and the quantification of the fluorescence intensity of one single filament was subjected to some variability. Nevertheless, we estimate that, in our experimental conditions, only 30% of fluorescence was lost after 40 frames. This result gives opportunities for kinetics analysis and organelle tracking with tdLanYFP using STED microscopy.

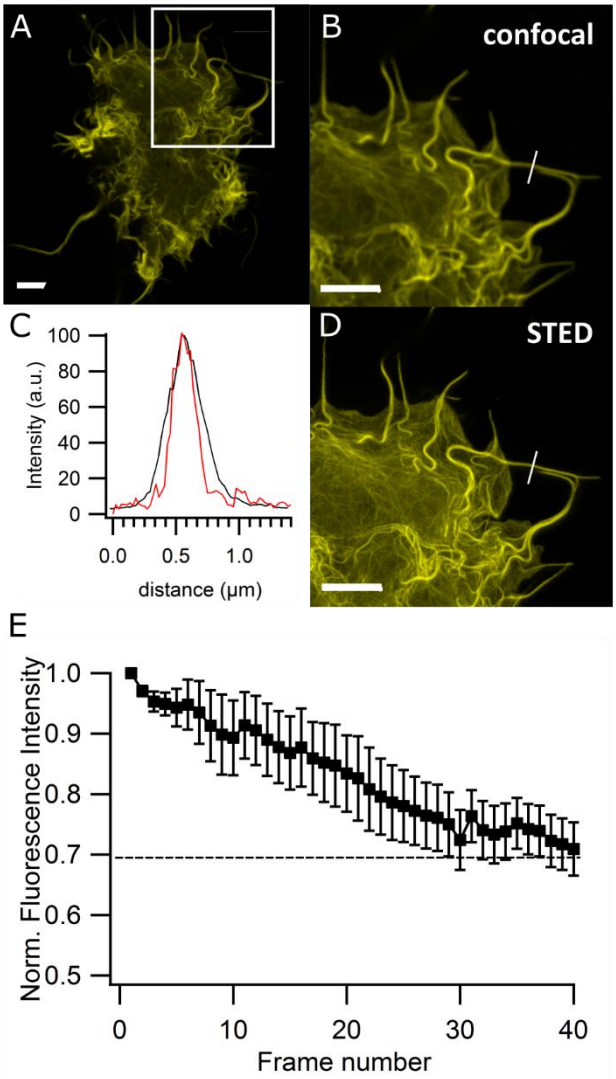

Figure 5: Confocal image of a whole COS7 cells expressing LifeAct-tdLanYFP (A), confocal and STED images of the white ROI (B, D). (C) Graph of the plots profile along the white line to show the gain in resolution. (E) Average of the fluorescence intensity decay in 5 ROIs along the actin filaments of the cell during a 40-frame time-lapse. Scale bars 5 µm.

The combination of high brightness with strong photostability is also particularly attractive for experiments in single molecule regimes. It is the case of fluorescence correlation spectroscopy (FCS), which monitors the diffusion of fluorescent molecules in and out of a confocal volume. At low expression levels, only a few molecules are probed in this volume. In the representative example showed in Figure 6, the fluctuations of the fluorescence intensity of cytosolic tdLanYFP were stable over 60 sec. In addition, the amplitude of the autocorrelation function (1/N), calculated from the fluorescence fluctuations, corresponds to N = 4 fluorophores. This gives a possibility to monitor the fluorescence of only a few molecules is the consequence of the high photostability of tdLanYFP, but it is also due to its improved brightness in comparison to the other YFPs. The tdLanYFP can thus be an option to overcome the weak photostability of

YFPs. Indeed, up to now there are only few examples of live-cell FCS experiments performed using YFP labels, despite their widespread use in live cell fluorescence imaging.

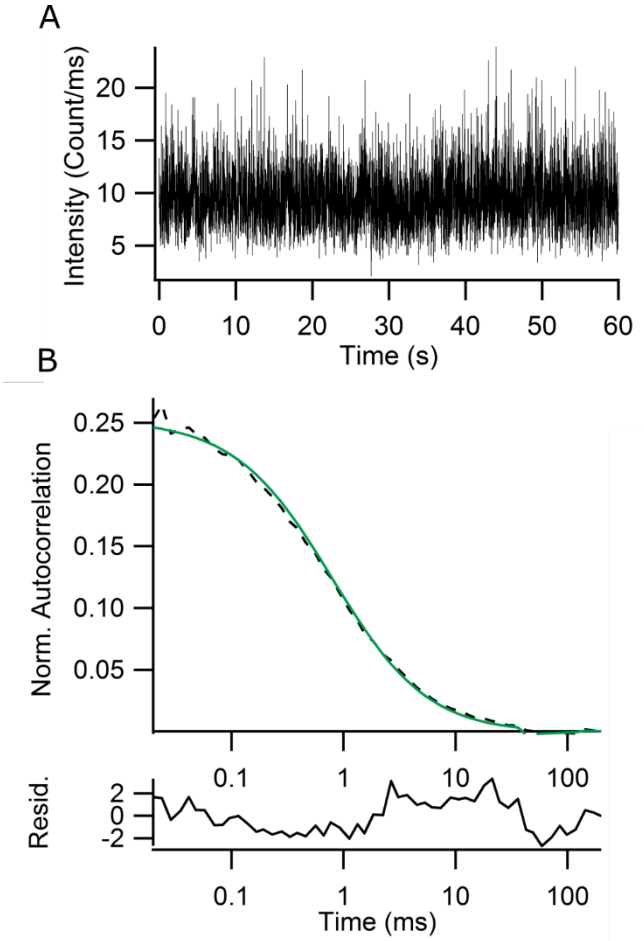

Figure 6: Fluctuations of fluorescence intensity (A) and the corresponding autocorrelation curve (B) acquired in the cytosol of one representative COS7 cell expressing cytosolic tdLanYFP. Experimental values are represented as the dashed line and their fit is in green. The residuals of the fit are displayed below the autocorrelation curve.

Full characterization of a model FRET system: Aquamarine-tdLanYFP FRET fusion

The theoretical Förster distance, R_0, at which the donor/acceptor FRET efficiency is 50 %, was calculated as 55 Å for the Aquamarine/dLanYFP monomer FRET pair (κ^2 =0,476 [3]). It is in the same order of magnitude as other CFP – YFP FRET pair (50-60 Å) and we decided to evaluate the possibility to use tdLanYFP as acceptor in FRET-based imaging applications. To this aim, we built a FRET fusion Aquamarine-tdLanYFP, and compared its response to the previously studied Aquamarine-Citrine fusion [19]. The two fusion constructs were similar, with the same donor (Aquamarine) separated from the acceptor with the same 27 residues linker and both expressed in COS7 cells. We monitored the lifetime of the donor by FLIM (Fig. 7) and also recorded the overall fluorescence spectra upon donor excitation in a field of view under the microscope (Fig. S6). The average lifetime of Aquamarine in the Aquamarine-tdLanYFP FRET

fusion is significantly lower than the one of Aquamarine expressed alone showing a strong energy transfer from Aquamarine to tdLanYFP, and giving an average FRET efficiency of 28 % (Fig. 7). This FRET is also clearly observed on the fluorescence spectrum through the presence of an intense fluorescence band between 520 and 530 nm characteristic of the acceptor fluorescence emission triggered by donor excitation and energy transfer (Fig. S6). The calculated FRET efficiency is similar to that observed in the original Aquamarine-Citrine construct (32%). This is rather surprising, considering that in the new Aquamarine-tdLanYFP construct, each Aquamarine donor is linked to two dLanYFP moieties, each with an increased extinction coefficient in comparison to Citrine. This might arise from an unfavorable relative orientation and distance of donor and acceptor chromophores in the FRET fusion. Alternatively, it might reflect the occurrence of dark, non-absorbing dLanYFP molecules, for example due to incomplete chromophore maturation.

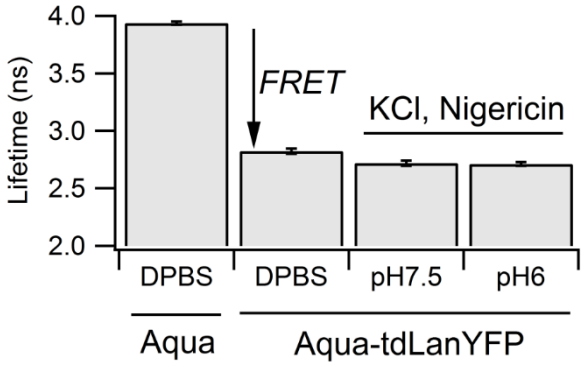

Figure 7: Fluorescence lifetimes of Aquamarine expressed in the cell cytosol of COS7 alone or in tandem with tdLanYFP at different pHs. Average of minimum 20 cells. Values displayed +/-SE.

As we observed a very low $pK_{1/2}$ for dLanYFP *in vitro* (Table 1), we also evaluated the effect of the pH on the FRET efficiency in the construct Aquamarine-tdLanYFP. The intra-cellular pH was fixed at pH 7.5 or pH 6 using a mixture of MES (15 mM) and HEPES (15 mM) buffers containing 140 mM KCl and 10 µM of an ionophore, the Nigericin. Within this pH range, Aquamarine's lifetime did not vary [7] and indeed, we observed the same donor lifetime for FRET fusion at both pHs (Fig. 7). This is an improvement compared to the Aquamarine / Citrine pair whose FRET efficiency changes in function of pH below pH 7 [19]. Indeed, acidic pHs induce the formation of the protonated form of Citrine whose absorption band, at lower wavelenghts than the deprotonated form, lead to a poor spectral overlay with the fluorescence emission spectrum of the donor [19]. As a consequence, the FRET pair Aquamarine / tdLanYFP is thus suitable for FRET studies at acidic pHs at least down to pH 6.

Applications of tdLanYFP as a FRET partner for live cell imaging

We further validated the use of tdLanYFP as FRET acceptor with Aquamarine as donor in a FRET biosensor reporting the autophosphorylation of protein kinase AURKA on Thr288[27]. The biosensor tdLanYFP-AURKA-Aquamarine was built, as well as a kinase-dead version that can not be phosphorylated on Thr288, tdLanYFP-AURKA(K162M)-Aquamarine as a control (Fig. 8A and B)[27]. We evaluated their responses by FRET/FLIM on the mitotic spindle in U2OS cells synchronized at mitosis, and in comparison to Aquamarine-AURKA as a lifetime reference. In the case of the AURKA kinase-responsive biosensor version, we observed a lifetime variation (ΔLifetime) of ~ 300 ps corresponding to the FRET from Aquamarine to tdLanYFP upon autophosphorylation on Thr288, a variation slightly higher than the value observed recently with the mTurquoise2/tdLanYFP FRET pair [27]. We also observed that the kinase-dead mutation K162M did not completely abolish FRET, neither did the small ATP analogue used to inhibit AURKA autophosphorylation, MLN8237. This was consistent with the observations done for the biosensor built with the mTurquoise2/tdLanYFP FRET pair [27]. As a rule of thumb, an efficient energy transfer can be observed up to twice R_0, the Förster distance. For Aquamarine/tdLanYFP and mTurquoise2/tdLanYFP FRET pairs, R_0 are in the 55-60 Å range. As for the AURKA kinase-responsive and kinase-dead version of the biosensor, the donor-acceptor distances were estimated to 83 Å and 97 Å respectively [27]. These two values are below twice R_0 (in a range between 110 Å and 120 Å) and therefore, FRET may be observed even within the more elongated inhibited or kinase-dead versions of the biosensor.

We also evaluated the possibility to use tdLanYFP as a FRET donor in intermolecular FRET. As a model, we used two subunits of the NADPH oxidase, $p67^{phox}$ and $p40^{phox}$ that are known to interact in the resting state of the enzyme [3]. The subunits were transiently expressed in COS7 cells and FRET was monitored by TCSPC-FLIM (Fig. 8C and D). The FRET efficiency was monitored using the lifetime of p67-tdLanYFP co-expressed with mCherry as a reference. We observed a significant decrease of the donor lifetime when the two protein partners, p67-tdLanYFP and mCherry-p40, were coexpressed (Fig 8C). For each cell, the FRET efficiency was plotted against $I_{Acceptor}$ (Fig. 8D). Interestingly, we noticed a non-specific FRET likely due to crowding that started even at the lowest analysed fluorescence intensities of the acceptor whether the FRET acceptor mCherry is fused to the $p40^{phox}$ subunit (black square, Fig. 8D) or not (empty circle, Fig. 8D). Nevertheless, the FRET efficiency for the co-expression of p67-tdLanYFP with mCherry-p40 was always above the control reaching a value of around 10 % for the highest fluorescence intensities of the acceptor consistantly with our previous

observations with the same proteins of interest [3]. This result validated tdLanYFP as donor in intermolecular FRET experiments.

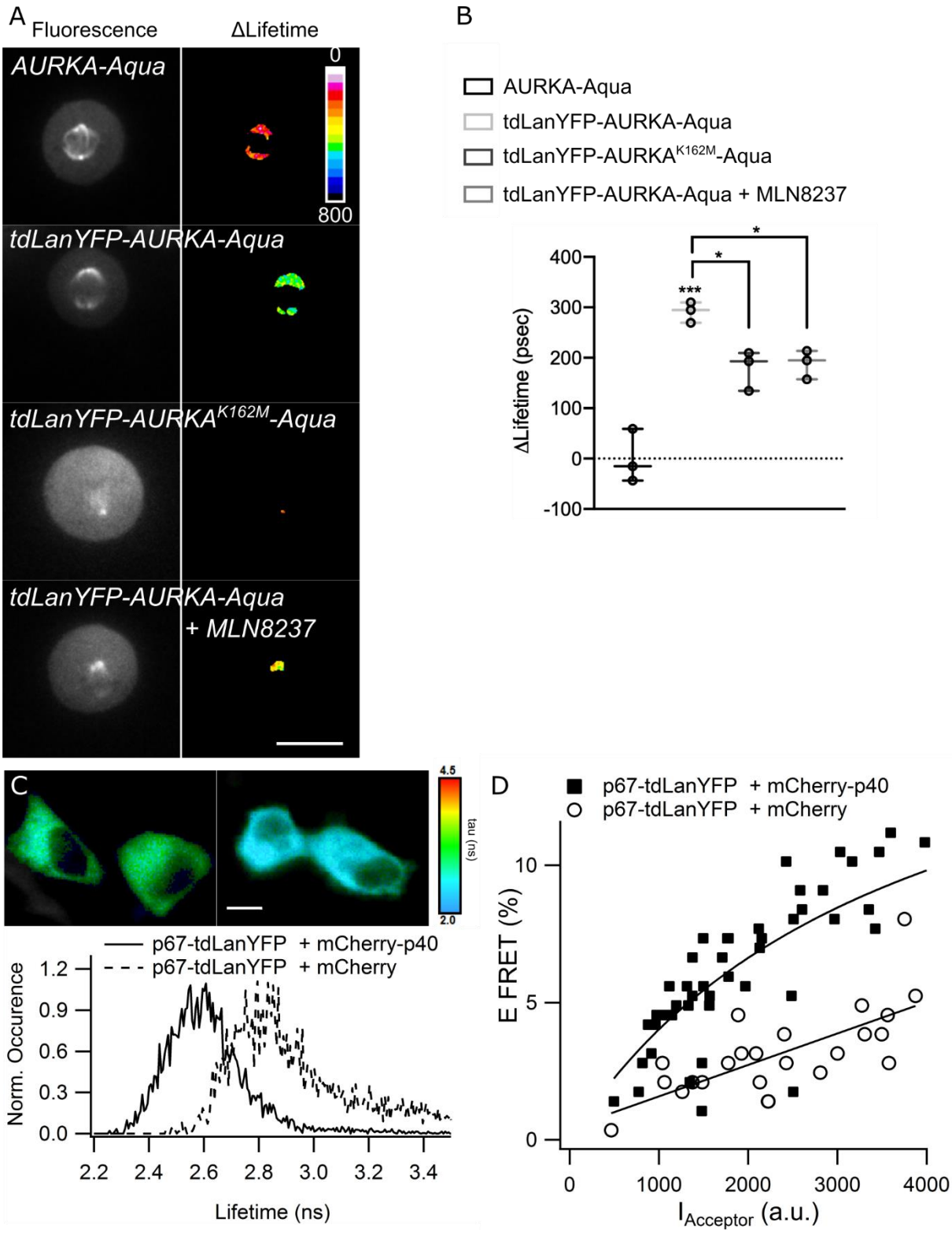

Figure 8: Representative fluorescence intensity (Aquamarine channel) and ΔLifetime images of U2OS cells expressing the indicated constructs and synchronized at mitosis (Scale bar 10 µm) (A) together with the corresponding ΔLifetime quantification at the mitotic spindle (B). The bar in boxplots represents the median; whiskers extend from the 10th to the 90th percentiles. Circles represent the mean FRET values issued by three independent experiments,

where 10 cells per experiment were analyzed. (C) Representative FLIM images of COS7 cells expressing p67-tdLanYFP with mCherry (left) or mCherry-p40 (right) and the corresponding lifetime histograms. Scale bar 10 μm. (D) Average FRET efficiencies plotted against acceptor (mCherry) fluorescence intensity. Each symbol represents the values for one cell. Solid line is for eye guidance only.

Conclusion

In this work, we have developed a high-performance yellow fluorescent protein for monitoring intracellular biological processes. tdLanYFP's performances surpass those of the currently available yellow fluorescent proteins and we show that this new FP can be used in various biosensing modalities.

In vitro, dLanYFP keeps most of the oustanding performances of the wild type LanYFP which are the best features for a yellow fluorescent protein including a brightness per chain 1.7 times higher than Citrine and a fluorescence lifetime of 2.9 ns. The tandem dimeric version, tdLanYFP, constructed for live cell experiments also allows most of the conventional imaging applications using the spectral selection available for conventional YFPs. Its photostability is a great advantage for applications requiring high-power illumination or long-time observations of a small pool of proteins, for example single molecule tracking or analysis of kinetics even in super-resolved imaging as STED microscopy. Its low $pK_{1/2}$ allows monitoring FRET at pH as low as 6 without any variation of FRET efficiency. This properties pave the way for new applications in acidic environements including the developpement of biosensors for the acidic degradative compartments of the endocytic and autophagic pathways or for the phagosomes, acidic traps of immune cells to destroy microbes. Those machineries are involved in many physio-pathological processes and moleculars tools such as genetically encoded biosensors are still missing mainly due to the lack of reliable FPs able to be a reliable optical reporter at acidic pHs. [12,28] Even though the tandem can now be used as it is in many applications, its relatively slow maturation could remain a drawback in particular for hetero-FRET application. This may be further improved by several rounds of mutagenesis. Nevertheless, the screening for fast-maturating versions of tdLanYFP should be performed while preserving the incredible brightness, excellent photostability and low pH-sensitivity of the current version of the protein.

Experimental part

Plasmid construction.

All details are provided in Supplementary Information.

In vitro expression and characterization of dLanYFP

For bacterial expression of dLanYFP, we used commercial plasmid pNCS-dLanYFP (Allele Biotechnology) to produce a 6xHis-tagged protein at its N-terminus. Competent TOP10 cells were transformed with the vector. A volume of 0.5 L of Luria–Bertani (LB) medium containing ampicillin (100 µg.mL^{-1}) was inoculated with a 25 mL starter culture that was grown overnight. After 18 h of culture at 30°C, bacteria were harvested by centrifugation (20 min, 5000 rpm) and frozen at -80°C. EYFP, Citrine and Venus were expressed as previously described [29]. The proteins were purified with our usual protocol without any modifications [29]. The concentrations of the proteins were measure biochemically with a BCA assay (Bicinchronic acid and copper from Sigma).

The absorption and fluorescence properties of purified proteins were studied at 22 °C in a 2 mM HEPES buffer or a 10 mM Tris H_2SO_4 buffer pH 8.0 at typically 10 µM concentration using a Lambda 750 spectrophotometer (Perkin Elmer) and Fluorolog 3 fluorimeter (Horiba). After a vertically polarized excitation at 515 nm (Δλ 2nm), fluorescence emission spectra were collected (Δλ 2nm) with the emission polarizer set at magic angle. After blank subtraction, the fluorescence spectra were corrected according to a transmission curve established using fluorescein in 0.1 M NaOH and rhodamine 6G in EtOH measured with the same set-up. [30,31]. Quantum yields were determined at 22°C by preparing a series of parallel dilutions of the protein and fluorescein at ODs ≤ 0.1, and comparing the slope *S* of their integrated corrected spectra as a function of dilution according to :

$$\phi_{FP} = \phi_{Ref} \frac{S_{FP}}{S_{ref}}$$

The reference quantum yield Φ_{Ref} of fluorescein in 0.1 M NaOH was taken as 0.925 [32].

The fluorescence lifetimes of the purified proteins were measured in a 10mM HEPES buffer pH 8 at typical 10 µM concentration and 20 ± 1°C using a TCSPC set-up previously described [33] and a picosecond pulsed excitation (20 MHz rep rate, P=4µW) from a white light FIANIUM source. The excitation was set at 515 nm (Δλ 5 nm) and fluorescence emission was collected at

535 nm (Δλ 9 nm). The instrumental response function was determined on a LUDOX solution setting the detection wavelength at 515 nm, and was used for reconvolution of analytical models and final comparison to experiments. After best curve fitting, chi-squares were comprised between 1.0 and 1.2 with randomly distributed residuals. In the case of tdLanYFP, the fluorescence lifetimes were obtained by global analysis of decays collected at 535 nm and 580 nm.

For the determination of $pK_{1/2}$, the spectra were recorded with a SynergyH1 plate reader (Biotek) in 96-transparent-well plates and spectra were processed as previously described [19]. Absorption spectra were recorded from 240 nm to 600 nm and fluorescence emission spectra from 500 nm to 700 nm upon excitation at 480 nm. For pH levels ranging from 11 to 5.5, buffer solutions contained 33 mM CAPS, 33 mM MES, and 33 mM Bis–tris propane and were adjusted to the appropriate pH by addition of H_2SO_4 or NaOH. For pH levels ranging from 5.5 to 2.5, buffer solutions consisted in 50 mM citric acid with appropriate volume of Na_2HPO_4 to adjust the pH. Aliquots from a concentrated stock protein solution were diluted into the different buffers at least 12 h before measurements. The concentration of chloride anion [Cl^-] was adjusted with a solution of concentrated KCl. Sodium gluconate was added to maintain a constant ionic force of 150 mM (except for the higher chloride concentrations, where no gluconate was added).

Maturation

The ability of newly synthetized dLanYFP to mature a fluorescent chromophore was studied in comparison to Citrine as a reference. Top10 bacteria were grown in their usual TB culture medium. In the case of dLanYFP, protein biosynthesis and fluorescence expression took place constitutively all along bacterial growth in LB medium. In the case of Citrine, protein expression in TOP10 cells were induced after prior cell growth to approximately 1 OD, by adding IPTG and ampicillin. Samples of the bacterial culture were collected at different times (typically every 30 min from 1 h to 5 h) after culture seeding (dLanYFP) or induction of protein expression (Citrine), centrifuged (20 min, 5000 rpm) and the cell pellets were immediately stored frozen at -80°C. On the day of experiments, pellets were thawed and cells were incubated under gentle agitation for 15 min in 2 mL of a lytic buffer (Lyse Cell Lytic B, Sigma in 40mM Tris-HCl pH8.0) containing 2mM PMSF as a protease inhibitor, followed by 2 min centrifugation at 15000 rpm. The progressive increase in fluorescence in the supernatant was then monitored using a SynergyH1 plate reader (Biotek). Kinetic traces followed a similar time

course independent of the sampling time of the bacterial culture for dLanYFP, while in the case of Citrine, the apparent fluorescence growth was progressively slower with increasing sampling time, which we ascribed to different levels of concurrent protease activity. Accordingly, only bacterial samples collected during the first two hours after induction were used. Averaged experimental results are presented Figure S6.

Live cells experiments

Most of the live cells experiments were performed in COS7. Cells were cultivated in DMEM Glutamax (Invitrogen) supplemented with 5 % FCS in 25 cm^2 flasks. For microscopy, cells were grown to 80 % confluence on glass coverslip (ibidi) and transiently transfected with the appropriate expression plasmids with XtremeGene HP (Roche Diagnostics) following the supplier's instructions and used 24–48 h after the transfection.[3] AURKA FRET biosensor was expressed in U2OS cells. The cells were cultivated, transfected and synchronized at mitosis as previously described. [27]

Microscopy

Wide field bleaching experiments were performed either on purified 6xHis-tagged fluorescent proteins attached to Ni-NTA agarose beads, or on COS7 cells expressing cytosolic constructs. In both cases, the epifluorescence pathway of the TCSPC-FLIM setup (see below) was used for illumination and fluorescence was excited and collected through a Semrock Brightline cube YFP-2427B-NTE-ZERO. The incident power on the sample was 530 µW and the diameter of the illumination field 400 µm, giving an approximate irradiance of 0.4W/cm^2. Averages of 5 to 10 individual intensity decay traces were collected for each sample type and fitted with single or double exponential decay models as required, from which the average bleaching time was computed.

For OSER assay, COS7 cells expressing the OSER construct of either tdLanYFP or Citrine targeted to the endoplasmic reticulum were imaged with an inverted Leica DMI8 microscope equipped with a 40x/0.6 NA objective (Leica) and piloted with Metamorph software. The epifluorescence pathway was equipped with a solid state light engine (Lumencor), a set of filter cubes and a CCD camera (Flash4.0LT, Hamamatsu Photonics). We used the Semrock Brightline cube YFP-2427B-NTE-ZERO for spectral selection. Images were analyzed visually using ImageJ. Typical examples of OSER cases are shown in Figure S5 for tdLanYFP (750 cells classified) and Citrine (420 cells classified).

Confocal images were acquired with an inverted Leica DMI 6000 microscope equipped with a 63x/1.4 NA PL APO oil immersion objective (Leica) and pilot with the LAS-X software (Leica). Excitation was performed at 510 nm with a white light laser and the fluorescence detected between 525 nm and 570 nm with a GaAsP Hybride detector (Hamamatsu).

For the photobleaching in confocal conditions and for STED imaging, LifeAct-mCitrine and LifeAct-tdLanYFP expressed in COS7 cells were imaged with an inverted Leica TCS SP8 gated-STED super-resolution microscope (Leica) equipped with a 100x/1.40 NA HCX PL APO STED oil immersion objective and piloted with the Leica SP8 LAS AF software (Version 3.6; Leica). The instrument was equipped with a WLL Laser (511 nm excitation wavelength) and a 592 nm depletion laser. The depletion laser was operated at an average power of 70 % of 400 mW with a gated detection of Tg = 1.5 ns-6 ns. The variations of the fluorescence intensities within the cells during the time-lapse over 30 frames in confocal imaging were measured in several ROIs in the cells and averaged. The final data are the average of 3 different cells.

For FCS experiments, an inverted Leica confocal microscope TCS SP8 SMD (Leica) was used. It was equipped with a DMI 6000 CS stand and a 63x/1.2 NA HC PLAN APO water immersion objective. The samples were excited with a continuous argon laser at 514 nm and the fluorescence was selected by 505 nm dichroic mirror and a bandpass filter BP 540/30 nm with an APD detector (PicoQuant). For the detection, the SMD module was constituted of a PicoHarp 3000 system for TTTR mode of single photon counting (PicoQuant). The fluctuations of fluorescence intensity were auto-correlated, and the resulting curves were analyzed using a standard pure diffusion model with SymphoTime (PicoQuant).

Fast-FLIM measurements were performed on a Leica DMI6000 microscope (Leica) equipped 63x/1.4 NA oil immersion objective and a time-gated custom-built setup for FLIM [34] and driven by the Inscoper hardware (Inscoper). Briefly, cells were excited at 440 ± 10 nm a using a white light pulsed laser (Fianium), and emission was selected using a band-pass filter of 483/35 nm. The detection is time-gated and the fluorescence lifetime was calculated with five sequential temporal gates of 2.2 ns each. The mean pixel-by-pixel lifetime was calculated only when the fluorescence intensity was above 3000 gray values using the Inscoper software (Inscoper). To calculate the ΔLifetime, the mean lifetime of the cells expressing the donor alone (AURKA-

Aquamarine) was calculated and its value was used to normalize data in all the analyzed conditions for each experiment.

TCSPC-FLIM microscopy was performed using a custom made time-resolved laser scanning TCSPC microscope described previously.[7] Briefly, the setup is based on a TE2000 microscope with a 60x, 1.2NA water immersion objective (Nikon). The epifluorescence pathway was equipped with a solid state light engine (Lumencor), a set of filter cubes and a CCD camera (ORCA AG, Hamamatsu Photonics). The spectral selections for CFP, YFP and RFP are available Table S1. The CFP cube was used for Aquamarine, the YFP cube for EYFP, Citrine, dLanYFP and tdLanYFP, the RFP cube for mCherry. A spectrometer (Ocean Optics) was fixed on the front exit of the microscope with an optical fiber. Emission spectra were recorded with the CFP excitation filter on the whole field of view (Fig. S6). The TCSPC path was equipped with a 440 and a 466 nm pulsed laser diode (PicoQuant) driven by a PDL800 driver (20 MHz, PicoQuant) for CFP and YFP respectively. The fluorescence was selected by a set of filters (Table S2) before the MCP-PMT detector (Hamamatsu Photonics). The C1 scanning head (Nikon) probed a 100µm x100µm field of view. The PicoHarp300 TCSPC module (PicoQuant) collected all the signals and data were processed with the SymPhoTime64 software (PicoQuant). The TCSPC fluorescence decay of all the pixels of the cytosol was computed by the SymPhoTime64 and decays were fitted with exponential fit functions:

$$I(t) = Background + I_0 \times \sum_i \alpha_i \, e^{-\frac{t}{\tau_i}}$$

The quality of the fit was evaluated by the weighted residual distribution and Pearson's χ^2 test. The average lifetime was computed as $< \tau >= \sum_i \alpha_i \, \tau_i$ and the apparent FRET efficiency was calculated using $< \tau_{DA} >$, the average lifetime of the donor in presence of acceptor and τ_{Donor}, the lifetime of the donor alone:

$$E_{FRET} = 1 - \frac{< \tau_{DA} >}{\tau_{Donor}}$$

We observed a slight decrease of the donor lifetime when the fluorescence intensity of the acceptor, $I_{Acceptor}$, in the cell increased (Fig. S7). $I_{Acceptor}$ is directly proportional to the concentration of the tandems in the cell cytosol in the case of Figure S7. When their concentration increased, a hetero-molecular FRET between close tandem molecules can happen in addition to the intra-molecular one within the tandems leading to the observed concentration-dependent lifetime decrease[35]. In order to minimize the effect of the so-called molecular crowding on the intra-molecular FRET efficiency, we set a maximum limit for $I_{Acceptor}$ at which

the donor lifetime decreased less than 5 % ($I_{Acceptor}$ < 1000 a.u.) in the tandem experiment. In Figure 8, the non-specific FRET due to crowding was directly evaluated by comparing the evolution of FRET efficiencies in presence of mCherry only with the ones in presence of mCherry fused to p40, the interaction partner of p67.

References

(1) Greenwald, E. C.; Mehta, S.; Zhang, J. Genetically Encoded Fluorescent Biosensors Illuminate the Spatiotemporal Regulation of Signaling Networks. *Chem. Rev.* **2018**, *118* (24), 11707–11794.

(2) Padilla-Parra, S.; Tramier, M. FRET Microscopy in the Living Cell: Different Approaches, Strengths and Weaknesses. *Bioessays* **2012**, *34* (5), 369–376.

(3) Ziegler, C. S.; Bouchab, L.; Tramier, M.; Durand, D.; Fieschi, F.; Dupré-Crochet, S.; Mérola, F.; Nüße, O.; Erard, M. Quantitative Live-Cell Imaging and 3D Modeling Reveal Critical Functional Features in the Cytosolic Complex of Phagocyte NADPH Oxidase. *J. Biol. Chem.* **2019**, *294* (11), 3824–3836.

(4) Zhou, X.; Mehta, S.; Zhang, J. Genetically Encodable Fluorescent and Bioluminescent Biosensors Light Up Signaling Networks. *Trends in Biochemical Sciences* **2020**, *45* (10), 889–905.

(5) Mérola, F.; Fredj, A.; Betolngar, D.-B.; Ziegler, C.; Erard, M.; Pasquier, H. Newly Engineered Cyan Fluorescent Proteins with Enhanced Performances for Live Cell FRET Imaging. *Biotechnology Journal* **2014**, *9* (2), 180–191.

(6) Tsien, R. Y. The green fluorescent protein. *Annu. Rev. Biochem.* **1998**, *67* (1), 509–544.

(7) Erard, M.; Fredj, A.; Pasquier, H.; Beltolngar, D.-B.; Bousmah, Y.; Derrien, V.; Vincent, P.; Merola, F. Minimum Set of Mutations Needed to Optimize Cyan Fluorescent Proteins for Live Cell Imaging. *Mol. BioSyst.* **2013**, *9* (2), 258–267.

(8) Goedhart, J.; van Weeren, L.; Hink, M. A.; Vischer, N. O. E.; Jalink, K.; Gadella, T. W. J. Bright Cyan Fluorescent Protein Variants Identified by Fluorescence Lifetime Screening. *Nat Methods* **2010**, *7* (2), 137–139.

(9) Goedhart, J.; von Stetten, D.; Noirclerc-Savoye, M.; Lelimousin, M.; Joosen, L.; Hink, M. A.; van Weeren, L.; Gadella, T. W. J.; Royant, A. Structure-Guided Evolution of Cyan Fluorescent Proteins towards a Quantum Yield of 93%. *Nat Commun* **2012**, *3* (1), 751.

(10) Casey, J. R.; Grinstein, S.; Orlowski, J. Sensors and Regulators of Intracellular PH. *Nat Rev Mol Cell Biol* **2010**, *11* (1), 50–61.

(11) Poëa-Guyon, S.; Pasquier, H.; Mérola, F.; Morel, N.; Erard, M. The Enhanced Cyan Fluorescent Protein: A Sensitive PH Sensor for Fluorescence Lifetime Imaging. *Anal Bioanal Chem* **2013**, *405* (12), 3983–3987.

(12) Nault, L.; Bouchab, L.; Dupré-Crochet, S.; Nüße, O.; Erard, M. Environmental Effects on Reactive Oxygen Species Detection—Learning from the Phagosome. *Antioxidants & Redox Signaling* **2016**, *25* (10), 564–576.

(13) Griesbeck, O.; Baird, G. S.; Campbell, R. E.; Zacharias, D. A.; Tsien, R. Y. Reducing the Environmental Sensitivity of Yellow Fluorescent Protein: mechanism and applications. *J. Biol. Chem.* **2001**, *276* (31), 29188–29194.

(14) Zacharias, D. A. Partitioning of Lipid-Modified Monomeric GFPs into Membrane Microdomains of Live Cells. *Science* **2002**, *296* (5569), 913–916.

(15) Kremers, G.-J.; Goedhart, J.; van Munster, E. B.; Gadella, T. W. J. Cyan and Yellow Super Fluorescent Proteins with Improved Brightness, Protein Folding, and FRET Förster Radius. *Biochemistry* **2006**, *45* (21), 6570–6580.
(16) Wiens, M. D.; Hoffmann, F.; Chen, Y.; Campbell, R. E. Enhancing Fluorescent Protein Photostability through Robot-Assisted Photobleaching. *Integr. Biol.* **2018**, *10* (7), 419–428.
(17) Shaner, N. C.; Lambert, G. G.; Chammas, A.; Ni, Y.; Cranfill, P. J.; Baird, M. A.; Sell, B. R.; Allen, J. R.; Day, R. N.; Israelsson, M.; Davidson, M. W.; Wang, J. A Bright Monomeric Green Fluorescent Protein Derived from Branchiostoma Lanceolatum. *Nat Methods* **2013**, *10* (5), 407–409.
(18) Cranfill, P. J.; Sell, B. R.; Baird, M. A.; Allen, J. R.; Lavagnino, Z.; de Gruiter, H. M.; Kremers, G.-J.; Davidson, M. W.; Ustione, A.; Piston, D. W. Quantitative Assessment of Fluorescent Proteins. *Nat Methods* **2016**, *13* (7), 557–562.
(19) Betolngar, D.-B.; Erard, M.; Pasquier, H.; Bousmah, Y.; Diop-Sy, A.; Guiot, E.; Vincent, P.; Mérola, F. PH Sensitivity of FRET Reporters Based on Cyan and Yellow Fluorescent Proteins. *Anal Bioanal Chem* **2015**, *407* (14), 4183–4193.
(20) Clavel, D.; Gotthard, G.; von Stetten, D.; De Sanctis, D.; Pasquier, H.; Lambert, G. G.; Shaner, N. C.; Royant, A. Structural Analysis of the Bright Monomeric Yellow-Green Fluorescent Protein MNeonGreen Obtained by Directed Evolution. *Acta Crystallogr D Struct Biol* **2016**, *72* (12), 1298–1307.
(21) Bajar, B.; Wang, E.; Zhang, S.; Lin, M.; Chu, J. A Guide to Fluorescent Protein FRET Pairs. *Sensors* **2016**, *16* (9), 1488.
(22) Betolngar, D.-B.; Erard, M.; Pasquier, H.; Bousmah, Y.; Diop-Sy, A.; Guiot, E.; Vincent, P.; Mérola, F. PH Sensitivity of FRET Reporters Based on Cyan and Yellow Fluorescent Proteins. *Anal Bioanal Chem* **2015**, *407* (14), 4183–4193.
(23) Campbell, R. E.; Tour, O.; Palmer, A. E.; Steinbach, P. A.; Baird, G. S.; Zacharias, D. A.; Tsien, R. Y. A Monomeric Red Fluorescent Protein. *Proceedings of the National Academy of Sciences* **2002**, *99* (12), 7877–7882.
(24) Shaner, N. C.; Campbell, R. E.; Steinbach, P. A.; Giepmans, B. N. G.; Palmer, A. E.; Tsien, R. Y. Improved Monomeric Red, Orange and Yellow Fluorescent Proteins Derived from Discosoma Sp. Red Fluorescent Protein. *Nat Biotechnol* **2004**, *22* (12), 1567–1572.
(25) Costantini, L. M.; Fossati, M.; Francolini, M.; Snapp, E. L. Assessing the Tendency of Fluorescent Proteins to Oligomerize Under Physiologic Conditions: Fluorescent Protein Oligomerization Assay. *Traffic* **2012**, *13* (5), 643–649.
(26) Valenta, H.; Erard, M.; Dupré-Crochet, S.; Nüβe, O. The NADPH Oxidase and the Phagosome. In *Molecular and Cellular Biology of Phagocytosis*; Hallett, M. B., Ed.; Advances in Experimental Medicine and Biology; Springer International Publishing: Cham, 2020; Vol. 1246, pp 153–177.
(27) Bertolin, G.; Sizaire, F.; Déméautis, C.; Chapuis, C.; Mérola, F.; Erard, M.; Tramier, M. Optimized FRET Pairs and Quantification Approaches To Detect the Activation of Aurora Kinase A at Mitosis. *ACS Sens.* **2019**, *4* (8), 2018–2027.
(28) Lie, P. P. Y.; Nixon, R. A. Lysosome Trafficking and Signaling in Health and Neurodegenerative Diseases. *Neurobiology of Disease* **2019**, *122*, 94–105.
(29) Alvarez, L.; Levin, C. H.; Merola, F.; Bizouarn, T.; Pasquier, H.; Baciou, L.; Rusconi, F.; Erard, M. Are the Fluorescent Properties of the Cyan Fluorescent Protein Sensitive to Conditions of Oxidative Stress? *Photochemistry and Photobiology* **2010**, *86* (1), 55–61.

(30) Porrès, L.; Holland, A.; Pålsson, L.-O.; Monkman, A. P.; Kemp, C.; Beeby, A. Absolute Measurements of Photoluminescence Quantum Yields of Solutions Using an Integrating Sphere. *Journal of Fluorescence* **2006**, *16* (2), 267–273.
(31) Kubin, R. F.; Fletcher, A. N. Fluorescence Quantum Yields of Some Rhodamine Dyes. *Journal of Luminescence* **1982**, *27* (4), 455–462.
(32) Magde, D.; Wong, R.; Seybold, P. G. Fluorescence Quantum Yields and Their Relation to Lifetimes of Rhodamine 6G and Fluorescein in Nine Solvents: Improved Absolute Standards for Quantum Yields. *Photochemistry and Photobiology* **2002**, *75* (4), 327–334.
(33) Villoing, A.; Ridhoir, M.; Cinquin, B.; Erard, M.; Alvarez, L.; Vallverdu, G.; Pernot, P.; Grailhe, R.; Mérola, F.; Pasquier, H. Complex Fluorescence of the Cyan Fluorescent Protein: Comparisons with the H148D Variant and Consequences for Quantitative Cell Imaging [†]. *Biochemistry* **2008**, *47* (47), 12483–12492.
(34) Bertolin, G.; Sizaire, F.; Herbomel, G.; Reboutier, D.; Prigent, C.; Tramier, M. A FRET Biosensor Reveals Spatiotemporal Activation and Functions of Aurora Kinase A in Living Cells. *Nat Commun* **2016**, *7* (1), 12674.
(35) Grailhe, R.; Merola, F.; Ridard, J.; Couvignou, S.; Le Poupon, C.; Changeux, J.-P.; Laguitton-Pasquier, H. Monitoring Protein Interactions in the Living Cell Through the Fluorescence Decays of the Cyan Fluorescent Protein. *Chem. Eur. J. of Chem. Phys.* **2006**, *7* (7), 1442–1454.